Original Article | **Open Access**

Carbon Footprints

Pan *et al*. *Carbon Footprints* **2026**, *5*, 52 **DOI:**10.20517/cf.2026.62

A novel allocation method and critical transport distance for industrial by-products in concrete

Lei Pan[1,2], Yuanfeng Wang[2], Yufang Fu[1], Boqun Zhang[2], Xiaohui Guo[3], Chengcheng Shi[4], Yinshan Liu[5], Liping Wang[2], Shaoqin Xue[2], Xinlei Chang[2], Xiaodong Liu[2]

Keywords: Industrial by-products, fly ash concrete, environmental impacts allocation principle, carbon footprint, life cycle assessment

Citation: Pan, L.; Wang, Y.; Fu, Y.; Zhang, B.; Guo, X.; Shi, C.; Liu, Y.; Wang, L.; Xue, S.; Chang, X.; Liu, X. A novel allocation method and critical transport distance for industrial by-products in concrete. *Carbon Footprints* **2026**, *5*, 52. https://dx.doi.org/10.20517/cf.2026.62

Received: 26 May 2026
First Decision: 22 Jul 2026
Revised: 2 Aug 2026
Accepted: 17 Aug 2026
Published: 23 Sep 2026

Academic Editors: Weina Meng, Kathleen B. Aviso
Copy Editor: Shu-Yuan Duan
Production Editor: Shu-Yuan Duan

Check for updates

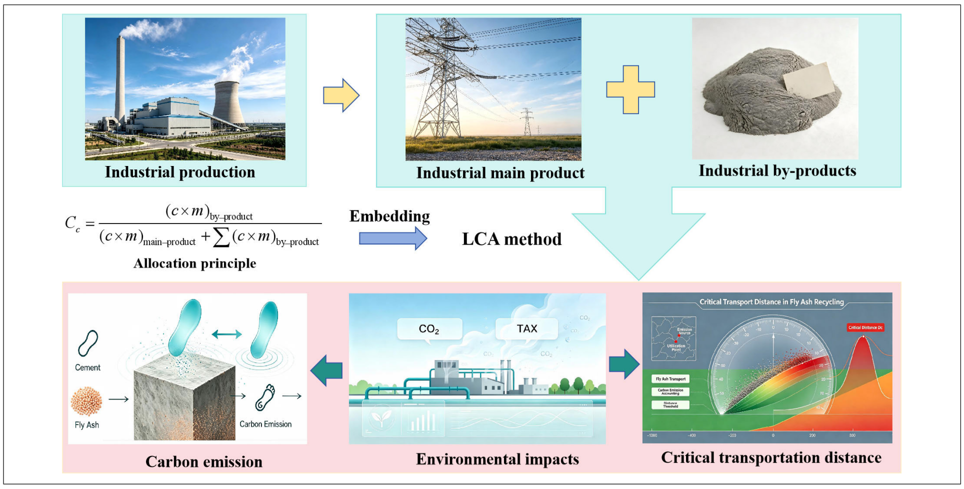

Abstract

Cement production accounts for about 8% of global CO_2 emissions, making it the largest industrial source in the construction material chain. Replacing cement with industrial by-products (IBPs) in concrete is a core pathway to reducing carbon footprint, but a scientifically sound allocation method is essential for accurately quantifying the carbon reduction contribution of IBPs. At present, the mainstream allocation methods in this field suffer from significant spatial and temporal fluctuations and low accounting stability, which seriously interfere with the accurate assessment of the carbon footprint and carbon emission reduction benefits of concrete incorporating IBPs. This study established an innovative production cost-based economic allocation principle for IBPs carbon footprints, which takes the manufacturing costs of primary industrial products and associated IBPs as the allocation core and considers their operational linkages within the industrial chain. Meanwhile, based on 929 groups of fly ash (FAH) concrete mix proportion data, a life cycle assessment approach was employed to systematically evaluate the carbon footprint characteristics of FAH concrete and quantify its critical transport distances (CTD). The

[1]Research & Innovation Center, Research Institute of Highway Ministry of Transport, Beijing 100088, China.
[2]School of Civil Engineering, Beijing Jiaotong University, Beijing 100044, China.
[3]China Petroleum International Pipeline Co., Ltd., Beijing 102200, China.
[4]School of Management, Tianjin University of Commerce, Tianjin 300134, China.
[5]Institutes of Science and Development, Chinese Academy of Sciences, Beijing 100190, China.

Correspondence to: Yuanfeng Wang, School of Civil Engineering, Beijing Jiaotong University, Beijing 100044, China. E-mail: cyfwang@bjtu.edu.cn

findings indicate that the environmental impacts allocation principle and concrete mix design dominate the carbon footprint reduction potential and CTD of FAH. Low-carbon transportation equipment can significantly expand FAH's CTD by reducing transport-related carbon footprint, which provides a scientific basis for the rational planning of large-scale promotion and efficient utilization of FAH. The proposed method offers a transferable methodological framework and may be adapted for carbon footprint accounting and carbon emission reduction contribution evaluation of other IBPs.

INTRODUCTION

Industrial by-products (IBPs) are non-primary outputs generated during industrial processes, with substantial production volumes. For instance, China alone produces approximately 600 million tons of fly ash (FAH) annually[1]. Improper management of these IBPs can lead to land occupation, soil and water contamination, air pollution, as well as resource depletion and energy inefficiency. However, through resource utilization, these IBPs can be transformed into high-value building materials, which not only eliminate environmental pollution but also reduce the carbon footprint over the whole life cycle of building materials, lower enterprise production costs, create economic value, and boost industrial technological innovation[2-5]. More importantly, the resource utilization of IBPs is a key path to reducing the carbon footprint of construction engineering, a core strategy for achieving circular economy and low-carbon development, and a critical support for advancing global sustainable development goals and building a resource-efficient, low-carbon, and environment-friendly society.

Concrete, the most widely used construction material globally, is highly energy-intensive and carries a huge carbon footprint throughout its production chain, with cement manufacturing being the dominant emission source[6-8]. According to research, producing one ton of cement emits approximately 0.85 ~ 0.92 tCO_{2eq}[9], with the cement sector contributing about 8% of total human-caused carbon emissions[10,11]. This oversized carbon footprint has become a major bottleneck restricting the sustainable development of the concrete industry. Using pozzolanic IBPs as supplementary cementitious materials (SCMs)[12-14] to partially replace cement is the most technically mature and economically feasible strategy to reduce the concrete carbon footprint and achieve substantial carbon reduction[15-18].

Multiple studies confirm that clinker substitution with SCMs reduces the carbon footprint of concrete by over 30%[19]. Singh and Prasad[20] reported that 65% FAH replacement reduces concrete carbon footprint by 54%. Orozco *et al.*[21] noted that 10%/15%/20% FAH replacement yields concrete carbon footprint reductions of 8.5% ~ 9.4%/8.5% ~ 20.7%/2.4% ~ 19.2%. Jiang *et al.*[22] pointed out that compared with ordinary concrete, a well-designed FAH concrete mix proportion can reduce its carbon footprint by up to 60.3%. Liao *et al.*[23] presented that when cement was completely replaced by FAH, the carbon footprint of FAH concrete was 7.9% ~ 21.2% lower than that of ordinary concrete. Li *et al.*[24] found that for alkali-activated slag-FAH concrete, when the strength grade is C30, the carbon footprint was reduced by 77.3% ~ 80.7%; when the strength grade is C50, the carbon footprint was reduced by 76.9% ~ 81.3%. Orozco *et al.*[25] verified that 25%/50% FAH replacement lowers the carbon footprint by 22% ~ 30.6%/44% ~ 51.4%. These data fully demonstrate that FAH concrete makes an outstanding contribution to carbon footprint reduction in the decarbonization of building materials.

Long-distance transportation can generate additional carbon emissions[26], which may gradually offset the carbon emission reduction benefits brought by FAH replacement. High-volume FAH mixes may even have a higher full-cycle carbon footprint than conventional concrete. This highlights that transport-related carbon footprint is a key factor restricting the carbon emission reduction contribution of SCMs. Jamora *et al.*[27] calculated that the critical transportation distance of FAH was 2841 km, beyond which the carbon footprint advantage of FAH concrete would disappear. O'Brien *et al.*[28] reported FAH's CTD (11,000km ~ 54,000 km), influenced by carbon footprint differences among transport modes. Bajpai *et al.*[29] found a CTD of 3219.27 km, beyond which the carbon footprint of FAH concrete exceeds that of conventional concrete.

The EU Waste Directive of 2008 stipulates certain conditions that materials must meet in order to be regarded as IBPs rather than waste[30]. Chen *et al.*[31] studied according to this directive and showed that FAH meets all the conditions for being an IBP and thus should not be regarded as waste. Therefore, when FAH is used as a cement substitute, its full-chain carbon footprint must be rigorously quantified, and its carbon emission reduction contribution must be accurately evaluated.

The life cycle assessment (LCA) results of green concrete carbon footprint strongly depend on the environmental impacts allocation principles of the modeled SCMs[32]. Currently, three primary methods are widely used: mass-based, economic, and no allocation[31]. Hafez *et al.*[33] reviewed 59 green concrete LCA papers and found that only 14 addressed allocation, with 8 using economic and 6 combining mass/economic approaches. Hossain *et al.*[15] reviewed LCA studies on concrete production using SCMs to replace cement over a decade and found that approximately 78% of the studies chose "no allocation", and approximately 37% chose the economic allocation principle. They emphasized the limitations of economic allocation due to temporal and spatial price volatility. Common allocation approaches can be found in Reference[15].

Even under the same allocation principle, carbon footprint calculation results vary greatly among researchers. For example, Chen *et al.*[31] presented that when the mass/economic allocation principles are selected, the environmental impacts allocation coefficients of FAH are 12.4% and 1%, respectively, and the carbon footprint per unit mass of FAH is approximately 495% and 41% of that of ordinary Portland cement, respectively. Zhang[34] provided the localized environmental impacts allocation coefficients of FAH in China. When the mass/economic allocation principles are selected, the environmental impacts allocation coefficients of FAH are 21.5% and 1%, respectively, and the carbon footprint per unit mass of FAH is approximately 174% and 8.1% of that of cement. Hossain *et al.*[15] obtained FAH allocation coefficients of 12.41% (mass allocation principle) and 2.18% (economic allocation principle), and the carbon footprint per unit mass of FAH is approximately 412% and 91% of that of cement. They further found that, relative to the economic allocation principle, applying the system-expansion-based allocation principle reduces the carbon footprint of SCM concrete by approximately 10% to 28%. This indicates that mass allocation methods result in considerably higher environmental impacts for concrete containing SCMs. Nevertheless, traditional economic allocation coefficients exhibit considerable temporal and spatial variability[31,35-37], resulting in unstable carbon footprint accounting and unreliable evaluation of carbon emission reduction benefits.

The divergent results reported in the literature reveal a critical contradiction in current allocation practices: the choice of allocation principle profoundly affects the assessed carbon footprint of SCMs, yet no consensus exists on which principle is most appropriate. The mass-based allocation, while physically transparent, tends to substantially overestimate the environmental burden of IBPs, thereby underestimating their carbon reduction contribution and discouraging their beneficial use. Conversely, the no-allocation approach, though maximizing the apparent benefit of IBPs, ignores the fact that IBPs are an integral output of the production system, thus failing to reflect their true environmental footprint. The traditional economic allocation, which attempts to balance these extremes by incorporating market values, introduces significant temporal and spatial volatility, leading to unstable and non-comparable results across different studies and regions. The deficiency of research lies in the lack of an allocation method that can simultaneously achieve theoretical rationality, result stability, and practical applicability. While system expansion has been proposed as an alternative, its application requires clear identification of substituted product systems, which is often complex and data-intensive[35-37].

Against this backdrop, the present study aims to fill this lack by proposing a novel allocation principle based on production costs - a parameter that is both economically meaningful and intrinsically stable. This method not only retains the economic rationale of value-based allocation but also overcomes the volatility inherent in market-price-based approaches. Using life cycle assessment, the present study analyzed the carbon footprint characteristics of FAH concrete and the CTD of FAH under different allocation principles, and clarified the carbon emission reduction contribution of FAH under multiple scenarios. The research results provide a theoretical foundation for accurate carbon footprint assessment and scientific carbon emission reduction potential evaluation of FAH resource utilization, and offer a methodologically transferable framework that, with appropriate adjustments, may be applicable to other IBP types for formulating targeted low-carbon development policies in the construction industry.

METHODS AND DATA

Traditional allocation principles

The environmental impacts (core: carbon footprint) of IBPs from production to final use can be expressed by:

$$I_i = C_j \times I_{\text{tei}} + I_{\text{sei}} + T_i \tag{1}$$

where I_i refers to the carbon footprint of IBPs i; C_j represents the carbon footprint allocation coefficient of the jth allocation method; I_{tei} and I_{sei} denote the total production impact, and the secondary processing impact, respectively; T_i stands for the carbon footprint generated when IBPs are transported to the place of use, which is not included when calculating the carbon footprint factor of IBPs.

Mass allocation principle

The no-allocation principle (C_0) treats waste as valueless, exempting it from primary production carbon footprint. However, valuable IBPs need to share part of this burden. Mass-based allocation (C_m) distributes carbon footprint proportionally to mass, as given in[31]:

$$C_m = \frac{m_{\text{by-product}}}{m_{\text{main-product}} + \sum m_{\text{by-product}}} \tag{2}$$

where C_m represents mass allocation coefficient; $m_{\text{main-product}}$ and $m_{\text{by-product}}$ refer to the mass of industrial main product and IBPs, respectively.

As indicated in the introduction, the carbon footprint of IBPs derived from mass allocation is significantly overestimated, which underestimates the carbon emission reduction contribution of IBPs and is unfavorable for their promotion. Therefore, this principle was excluded from subsequent analysis.

Economic allocation principle

To better allocate the environmental impacts of IBPs, Chen *et al.*[31] proposed the traditional economic allocation principle (C_e), which allocates carbon footprint via market prices, as given in:

$$C_e = \frac{(e \times m)_{\text{by-product}}}{(e \times m)_{\text{main-product}} + \sum (e \times m)_{\text{by-product}}} \tag{3}$$

where C_e stands for the carbon footprint allocation coefficient of IBPs based on the economic allocation principle; $e \times m$ represents production revenue.

Using Equation (3), the FAH's carbon footprint allocation coefficient was 5.31%. The production volume, production cost, cost composition, and data sources used for calculation all come from the literature[38]. This coefficient is then applied to the total production impact via Equation (1), yielding the carbon footprint factor of 303.81 $kgCO_{2eq}$/t for FAH under the traditional economic allocation principle.

New economic allocation principle

The production cost of a product encompasses all production expenses incurred by an enterprise during the production process. It represents the capital outlay that the enterprise advances in anticipation of generating revenue. The production cost of the product is composed of three components: direct materials, direct labor, and manufacturing overhead. Direct materials refer to the raw materials that form the physical substance of the product, along with the primary and auxiliary materials that facilitate product formation. Direct labor denotes the employee compensation of workers engaged in product manufacturing. Manufacturing overhead consists of various indirect costs incurred by the enterprise's production department for product manufacturing and service provision, including the consumption of machine supplies, the salaries of workshop management personnel, depreciation expenses, office expenses, and utility bills such as water and electricity charges.

Based on the production cost of products, a new economic allocation principle was proposed, as expressed by

$$C_c = \frac{(c \times m)_{\text{by-product}}}{(c \times m)_{\text{main-product}} + \sum (c \times m)_{\text{by-product}}} \quad (4)$$

where C_c is the carbon footprint allocation coefficient of IBPs based on the new economic allocation principle; $c \times m$ refers to total production cost.

The proposed method adopts production cost as an alternative economic basis for allocating environmental burdens to industrial IBPs. Its theoretical rationality rests on three aspects. First, in a multi-product system, the main product and the IBP are generated jointly within the same production process. Production cost-encompassing direct materials, direct labor, and manufacturing overhead-directly measures the resources actually invested by the enterprise to obtain each output. Compared with market prices, which are significantly influenced by supply-demand dynamics and policy interventions, production cost more genuinely reflects the "resource contribution" of the IBPs within the production system, thereby providing a more reasonable basis for determining its share of the environmental burden.

Second, the production-cost principle is intrinsically aligned with the "industrial-chain linkage" nature of IBPs. As clarified by the EU Waste Framework Directive, IBPs are an organic part of the production process. When IBPs are valorized, their environmental burden allocation should reflect their inherent connection with the main product. Using production cost rather than market value can accurately characterize this intrinsic industrial-chain relationship.

Third, the method is well compatible with the ISO 14044 framework. When system expansion or process subdivision is infeasible, ISO 14044 permits allocation based on parameters such as economic value. Our method is an improved variant of traditional economic allocation, replacing volatile market prices with more

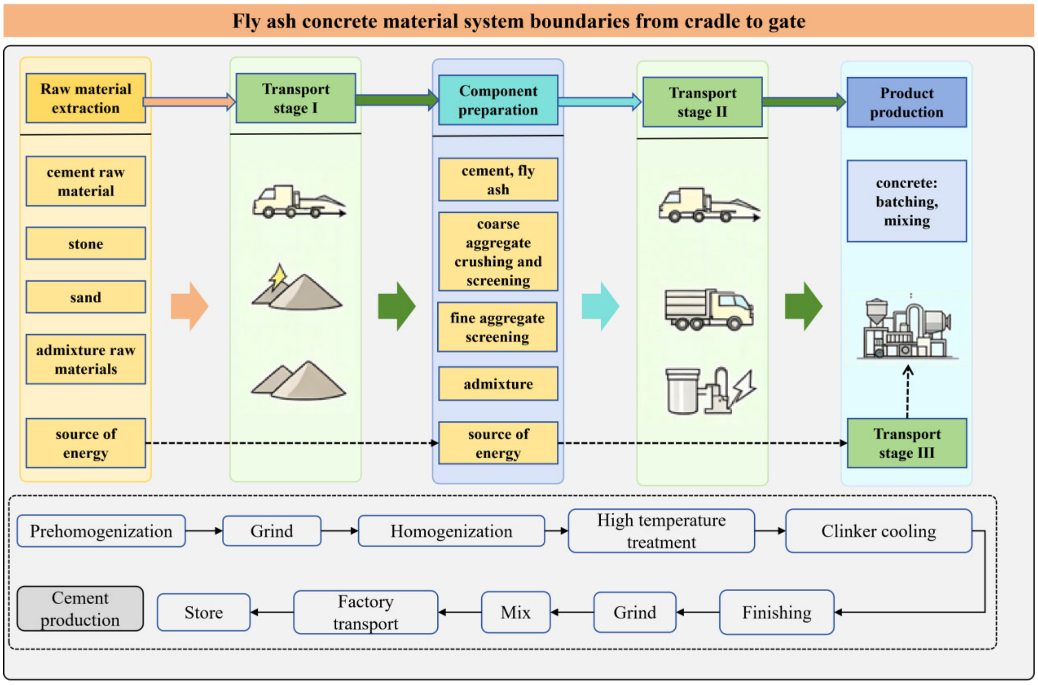

Figure 1. System boundary of FAH concrete. FAH: Fly ash.

stable production costs as the allocation basis.

Using Equation (4), the FAH's carbon footprint allocation coefficient was 1.94%. The production volume, production cost, cost composition, and data sources used for calculation all come from the literature[38]. This coefficient is then applied to the total production impact via Equation (1), yielding the carbon footprint factor of 115.11 $kgCO_{2eq}$/t for FAH under the new economic allocation principle. Cao *et al.*[39] have demonstrated that the volatility of the producer price index is significantly lower than that of the commodity price index. Therefore, the FAH allocation coefficient obtained by the new economic allocation principle has less volatility and better stability.

LCA method

ISO standards define four LCA phases: goal definition, inventory analysis, impact assessment, and interpretation[40,41]. Two functional units are adopted to capture different perspectives of carbon footprint performance: FU_1 ($kgCO_{2eq}/m^3$) represents the volumetric carbon footprint per cubic meter of concrete, while FU_2 (carbon footprint intensity,$kgCO_{2eq}/MPa/m^3$) normalizes the carbon footprint by compressive strength to account for the trade-off between environmental impact and mechanical performance. FU_2 is given in[34]

$$C_i = \frac{CO_{2eq}}{f_{c,28}} \quad \left(\mathrm{kgCO_{2\,eq}}/\mathrm{m}^3/\mathrm{MPa}\right) \tag{5}$$

The system boundary, as illustrated in Figure 1, encompasses all processes from raw material extraction to the concrete plant gate, following the "cradle-to-gate" approach.

The carbon footprint factors of the production process used for calculating the carbon footprint of FAH concrete were derived from literature[42-46], among which the carbon emission factor of Class 8b trucks is 0.104341 $kgCO_{2eq}$/(t·km). The transport distances for materials and energy at various stages were set [Table 1].

Table 1. Distance of material and energy transport at each stage

Transport stages	Materials or energy	Mode	Distance
Transport I/km	Cement raw materials to cement plant	Class 8b truck	40
	Gypsum to cement plant	Class 8b truck	40
	Sand to fine aggregate plant	Class 8b truck	10
	Rock to coarse aggregate plant	Class 8b truck	5
Transport II/km	Cement to concrete plant	Class 8b truck	176
	Fine aggregate to concrete plant	Class 8b truck	176
	Coarse aggregate to concrete plant	Class 8b truck	176
Transport III/km	Crude oil to energy processing plants	Pipeline	637
	Coal to coal-fired power plant	Class 8b truck	176
	Diesel, gasoline to the petrol station	Oil tank truck	176
	Diesel, gasoline to the product oil transfer center	Pipeline	637
	Electricity to the construction site	Line loss rate：4.84%	

Table 2. Groups with strengths and dosage ranges

Compressive strength (MPa)	Range							
	[30,40)		[40,50)	[50,60)	[60,70)	[70,80)		≥ 80
Number	449		311	178	144	88		86
Ratio (%)	35.75		24.76	14.17	11.46	7.01		6.85
FAH content (%)	Range							
	0	(0 ~ 10]	(10 ~ 20]	(20 ~ 30]	(30 ~ 40]	(40 ~ 50]	(50 ~ 60]	＞ 60
Number	327	94	248	229	160	107	65	26
Ratio (%)	26.04	7.48	19.75	18.23	12.74	8.52	5.18	2.07

FAH: Fly ash.

Table 3. Groups with strength classes

Class	C30	C35	C40	C45	C50	C55	C60	＞ C60
Number	225	224	186	125	96	82	99	219
Ratio (%)	17.91	17.83	14.81	9.95	7.64	6.53	7.88	17.44

Data collection

A dataset of 1256 concrete mix designs was compiled, consisting of 929 groups of FAH concrete (with FAH content > 0) and 327 groups of ordinary concrete (with FAH content = 0) as controls, categorized by 28-day compressive strength and FAH content [Table 2][30,47-64], providing a large dataset for accurate carbon footprint calculation and carbon reduction contribution evaluation[47-64]. The mix proportion data of all 1,256 concrete samples were grouped according to the compressive strength grade, as shown in Table 3. The data were screened according to the following criteria: (1) complete records of 28-day compressive strength and all mix proportion components (cement, FAH, water, aggregates, and admixtures); (2) clearly reported mix designs without missing critical parameters; and (3) test results obtained under standard curing conditions. No additional preprocessing such as data imputation or transformation was applied.

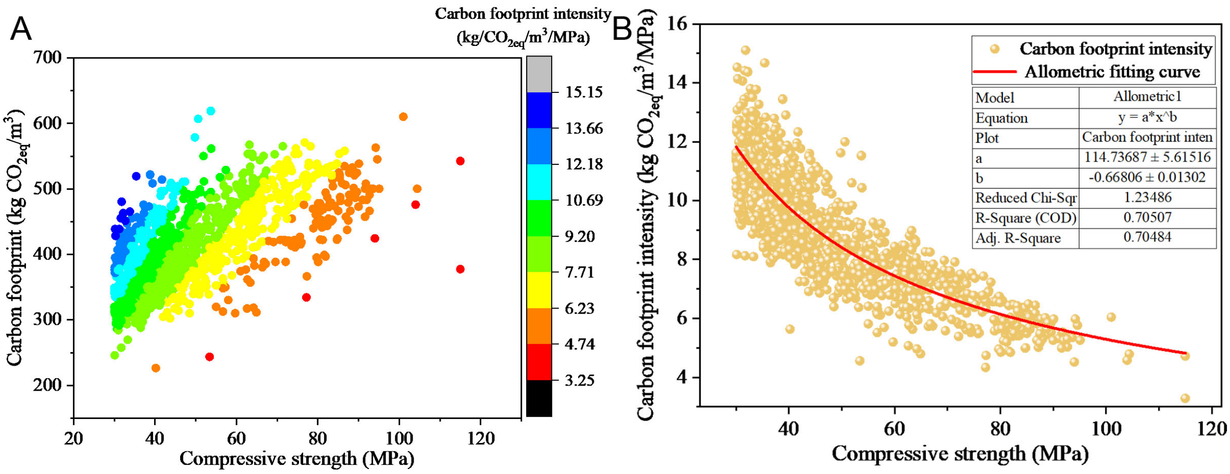

Figure 2. Carbon footprint and carbon footprint intensity. (A) Carbon footprint (FU_1) versus compressive strength; (B) Carbon footprint intensity (FU_2) versus compressive strength.

RESULTS AND ANALYSIS

Carbon footprint

Rapid estimation model

Under the C_0 allocation principle, Figure 2 illustrates the relationships between the compressive strength and the carbon footprint as well as carbon footprint intensity. For functional unit FU_1, the carbon footprint increases with higher compressive strength, whereas for FU_2, carbon footprint intensity decreases. Furthermore, the dispersion of carbon footprint intensity under FU_2 is lower than that of carbon footprint under FU_1.

Given the low variability of carbon footprint intensity, an allometric function was used for fitting, resulting in:

$$C_i = 114.74 f_{c,28}^{-0.068} \tag{6}$$

The carbon footprint per unit strength can be calculated using Equation (6) and the compressive strength, allowing rapid per-volume carbon footprint estimation and markedly improving efficiency.

Figure 3 illustrates the carbon footprint and carbon footprint intensity of FAH concrete under the C_e and C_c allocation principles. Regardless of the principle, the carbon footprint increases with strength under FU_1, while carbon footprint intensity decreases under FU_2, with lower dispersion than FU_1. The fitting formulas for carbon footprint intensity under each principle are listed in Table 4.

Carbon footprint characteristics

Based on the 929 sets of FAH concrete mix proportion data, carbon footprints were calculated under different allocation principles, and the corresponding statistical parameters were derived. These parameters include the maximum value ($C_{FU_1,\max}$), minimum value ($C_{FU_1,\min}$), median value ($\bar{C}_{FU_1}$), mean value (μ_{FU_1}), standard deviation (σ_{FU_1}), and variation coefficient (δ_{FU_1}) of the carbon footprint. Table 5 presents the calculation results.

Table 5 shows that, under any allocation principle, the mean and median carbon footprint of FAH concrete increase with strength grade. In contrast, the standard deviation and coefficient of variation exhibit notable

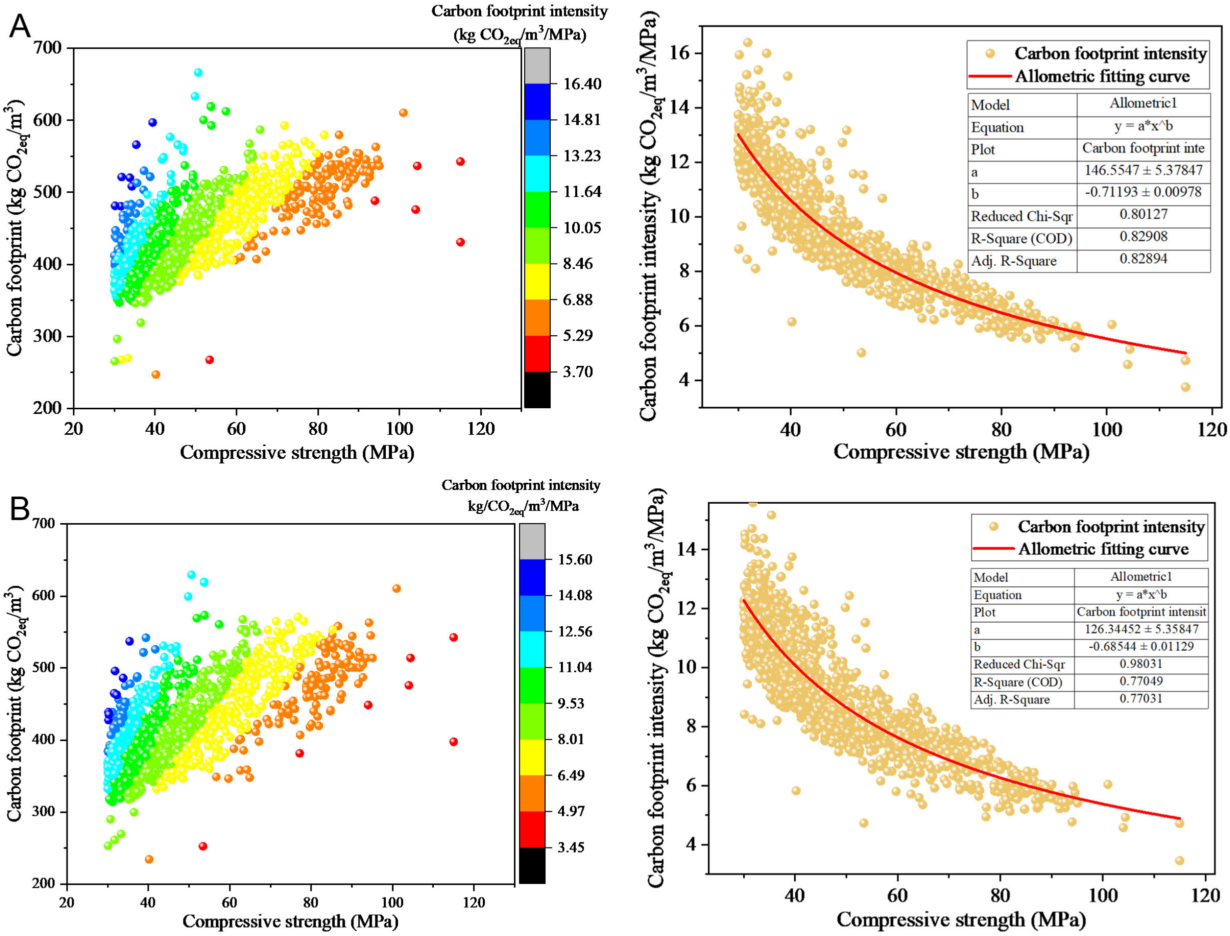

Figure 3. Carbon footprint and carbon footprint intensity. (A) Carbon footprint and carbon footprint intensity under the Ce allocation principle; (B) Carbon footprint and carbon footprint intensity under the C_c allocation principle.

Table 4. Carbon footprint intensity fitting formulas under different allocation principles

Allocation principle	Equation	R^2
C_e	$C_i = 146.55 f_{c,28}^{-0.712}$	0.8291
C_c	$C_i = 126.34 f_{c,28}^{-0.065}$	0.7705

variability across grades, with the highest values for C50. This variability also reflects the variation in carbon footprint caused by differing mix proportions within the same strength grade.

A violin plot is a statistical chart that combines the features of a box plot and a kernel density plot. It uses the box plot concept to display various percentiles of the data, while the kernel density plot is used to show the "contour" effect of the data distribution. The kernel density plot is usually displayed on both sides of the box plot, forming a shape similar to a violin. The larger the "contour", the more the data is concentrated in that area, and vice versa, indicating fewer data points in that area. Figure 4 illustrates the distribution of carbon footprint across different strength grades and allocation principles, clearly showing that the median carbon footprint increases with compressive strength grade, and the probability density peaks near the median.

Meanwhile, there is an "overlap" in the carbon footprint of different strength grades of FAH concrete, which is mainly attributable to two reasons. Firstly, since FAH is used as an SCM to replace cement, the amount of

Table 5. Statistical parameters of carbon footprint

Allocation principle	Parameter	C30	C35	C40	C45	C50	C55	C60	> C60
C_0	$C_{FU_1,\max}$	480.46	522.02	514.32	578.72	619.40	528.99	567.58	610.38
	$C_{FU_1,\min}$	245.90	287.86	226.45	310.26	243.51	310.26	311.44	334.31
	$\bar{C}_{FU_1}$	368.76	380.33	388.56	397.23	416.65	433.96	462.12	487.88
	$\mu_{C_{FU_1}}$	366.87	381.61	395.20	408.00	429.40	432.76	460.11	485.10
	$\sigma_{C_{FU_1}}$	44.22	48.76	50.09	52.36	67.01	48.99	52.99	45.49
	$\delta_{C_{FU_1}}$	12.05%	12.78%	12.67%	12.83%	15.61%	11.32%	11.52%	9.38%
C_e	$C_{FU_1,\max}$	521.20	597.02	576.66	633.40	666.38	612.54	567.58	610.38
	$C_{FU_1,\min}$	265.35	318.94	246.99	376.30	267.42	400.01	407.14	417.82
	$\bar{C}_{FU_1}$	397.60	413.34	424.18	431.19	443.39	464.84	486.07	512.15
	$\mu_{C_{FU_1}}$	401.58	415.62	427.61	443.39	457.66	467.07	488.45	513.03
	$\sigma_{C_{FU_1}}$	36.78	37.33	41.43	46.92	59.02	34.19	33.90	30.98
	$\delta_{C_{FU_1}}$	9.16%	8.98%	9.69%	10.58%	12.90%	7.32%	6.94%	6.04%
C_c	$C_{FU_1,\max}$	495.90	542.03	530.85	599.44	629.58	560.64	567.58	610.38
	$C_{FU_1,\min}$	253.27	299.64	234.23	344.52	252.57	346.52	347.70	381.52
	$\bar{C}_{FU_1}$	380.63	394.12	399.89	411.66	427.55	444.97	469.95	499.56
	$\mu_{C_{FU_1}}$	380.02	394.50	407.48	421.41	440.11	445.76	470.85	495.68
	$\sigma_{C_{FU_1}}$	39.43	42.69	45.40	48.79	62.72	41.47	44.90	38.71
	$\delta_{C_{FU_1}}$	10.38%	10.82%	11.14%	11.58%	14.25%	9.30%	9.54%	7.81%

cement used is reduced, thereby reducing the carbon footprint. For example, when the strength grade of FAH concrete is C50 or even higher, owing to the different FAH contents, its carbon footprint may be lower than that of C30 concrete. Secondly, since the mix proportion determines the amounts of materials used, a good mix proportion can consume fewer materials while meeting the compressive strength requirements, thus reducing the carbon footprint. However, if the mix proportion is not optimal, the use of FAH may not reduce the carbon footprint. In some instances, the carbon footprint exceeds that of ordinary concrete with the same or even higher strength grades. This highlights the importance of mix proportion optimization. In addition, the properties of raw materials, construction procedures during the concrete production process, and the testing process can also increase the variability of carbon footprint of FAH concrete[30,34].

Critical transport distance

O'Brien *et al.*[28] noted that the transport distance of FAH greatly affects the environmental load of FAH concrete: longer distances gradually offset the environmental benefits of incorporating FAH. Therefore, analyzing the FAH's CTD is necessary. The CTD was calculated using the average carbon footprint of conventional concrete (0% FAH, i.e., the 327 control groups) at various strength grades as a reference. The critical transportation distance of FAH is shown in Equation (7), where the FAH content is greater than 0 (this study has 929 sets of data).

$$L_{\text{limit}}(i,j) = \frac{C_{FU_1-0\%} - \Delta C_{FU_1-C_i-FAH\%}}{2 \times EF_{T_j} \times m_{FAH}/1000} \tag{7}$$

where $L_{limit}(i,j)$ is the CTD for a given scenario; $C_{FU_1-0\%}$ is the reference carbon footprint at 0% FAH content; $\Delta C_{FU_1-C_i-FAH\%}$ represents the carbon footprint of concrete with different FAH dosages based on the principle of allocating the environmental impact of FAH, excluding all transportation stages of FAH; EF_{T_j} and m_{FAH} are the carbon footprint factor for a transport mode [kgCO_{2eq}/(t·km)] and the mass of FAH (kg). To account for environmental impacts from empty driving, the transport distance is doubled[65].

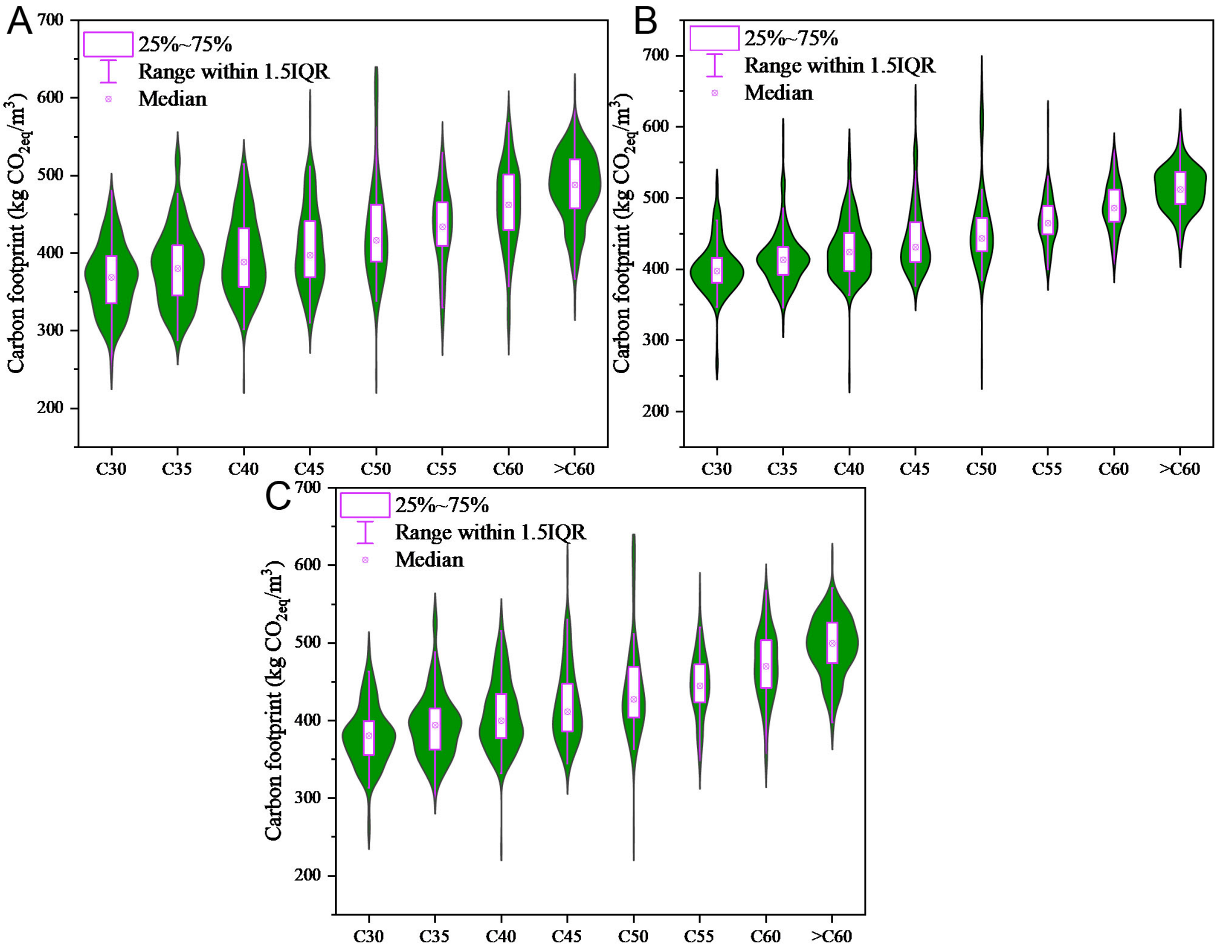

Figure 4. Carbon footprint distribution characteristics under different allocation principles. (A) Violin plot of carbon footprint distribution under the C_0 allocation principle; (B) Violin plot of carbon footprint distribution under the C_e allocation principle; (C) Violin plot of carbon footprint distribution under the C_c allocation principle. The green shaded regions represent the kernel density estimation contours, which indicate the probability density distribution of the carbon footprint data, the wider the green area, the more concentrated the data points at that value. IQR: Interquartile range.

The influence of mix proportion uncertainty on the CTD

Using Equation (7), the CTD of FAH was calculated for different strength grades of FAH concrete under various allocation principles. Figure 5 presents the CTD values for C30, C40, C50, and C60. In all strength grades, negative CTD values appear, particularly for lower grades such as C30 and C40, indicating that FAH application results in a higher carbon footprint than that of the reference scenario. This phenomenon primarily results from sub-optimal mix proportions, which cause higher material consumption and consequently offset the carbon reduction potential of FAH.

At lower FAH content levels, the CTD exhibits a wider distribution range, primarily due to uncertainties in mix proportion design. When an optimal FAH concrete mix proportion is achieved, the significant reduction in material usage leads to a substantially lower carbon footprint compared to the reference value. In calculating FAH's CTD using Equation (7), both the carbon emission reduction from material savings and FAH's inherent carbon emission reduction capability are considered as FAH's contribution. In this case, the mass of FAH is relatively small, which increases the CTD.

When cement is replaced by an equal mass of FAH without compromising concrete strength, the CTD of FAH increases as the FAH dosage rises. However, this is not the case in practice. High FAH content reduces

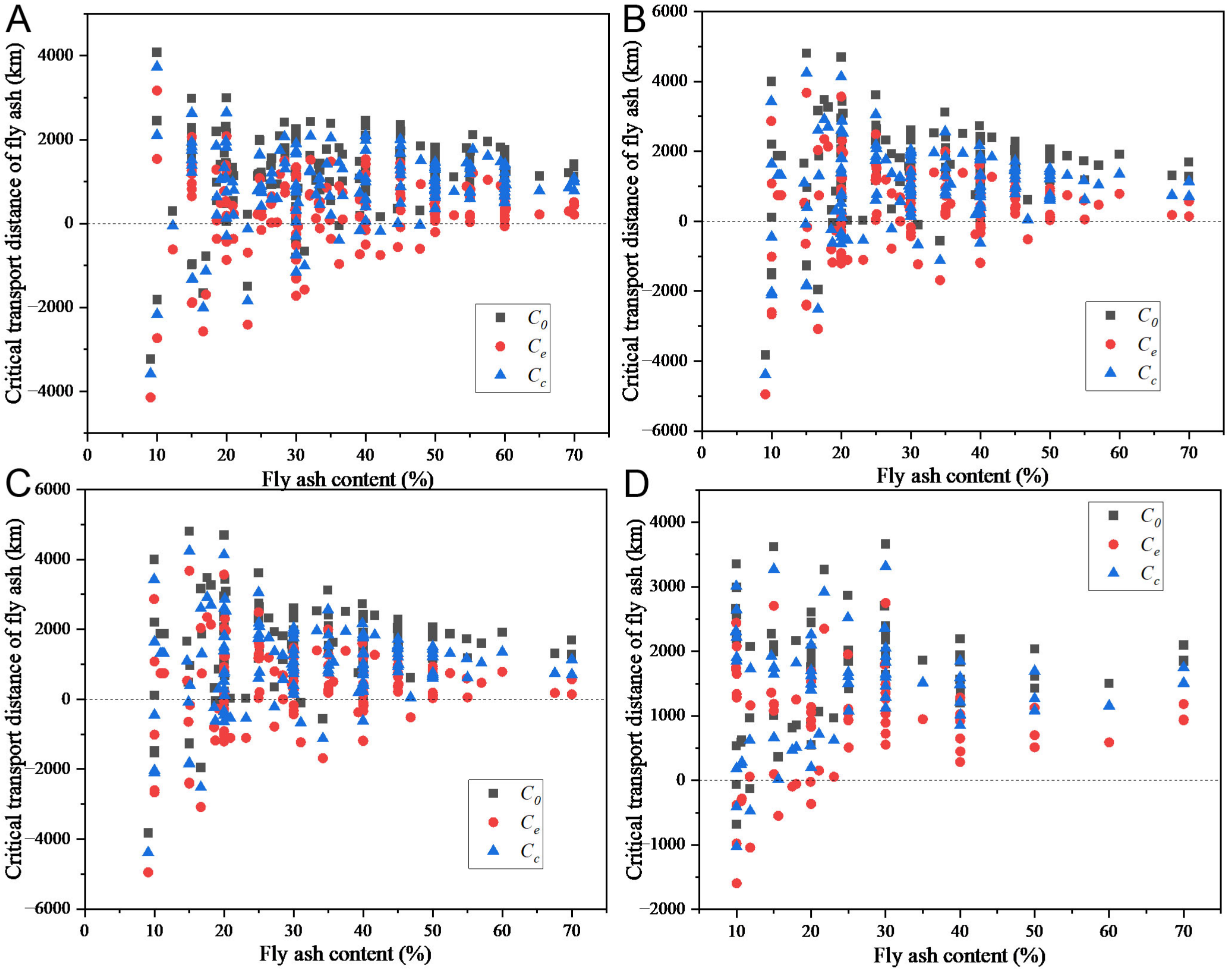

Figure 5. Critical transport distance of FAH. (A) CTD distribution for C30; (B) CTD distribution for C40; (C) CTD distribution for C50; (D)CTD distribution for C60. FAH: Fly ash; CTD: critical transport distance.

the compressive strength of concrete[66]. When additional cement or admixtures are needed to achieve the same strength grade, the carbon reduction advantage of FAH is reduced. Moreover, given the relatively large mass of FAH in this case, the CTD for FAH decreases. Furthermore, when a substantial amount of FAH is utilized, although the CTD would not become negative, there can be instances where the CTD is quite small. Most FAH comes from power plants, so it is often transported over long distances to concrete processing plants. A very short CTD causes FAH concrete's carbon footprint to surpass the reference value, making it difficult to meet carbon emission reduction goals. This also fully underscores that optimizing the mixing ratio is the key to carbon reduction, and even an indispensable step.

The CTD values for FAH concrete of various strength grades across all mix proportion schemes were averaged to obtain a statistically meaningful CTD for FAH, as illustrated in Figure 6. As shown in Figure 6, for all strength grades of FAH concrete, increasing the carbon footprint allocation coefficient raises the carbon footprint coefficient of FAH and reduces its CTD. Under the allocation principles of C_0, C_c, and C_e, when the strength grade of FAH concrete is C50, the CTD for FAH is the largest, measuring 1,992 km, 1,646 km, and 1,079 km, respectively. Next, for C35, the CTD values are 1811 km, 1,465 km, and 899 km, respectively. For C30, the values are the smallest, at 1,171 km, 825 km, and 259 km. Based on these, the unweighted average CTD across all strength grades under the C_0, C_c, and C_e allocation principles are 1,538 km, 1,166 km, and 599 km, respectively, with a maximum difference of 939 km. This fully demonstrates the significance of the environmental impact allocation principle.

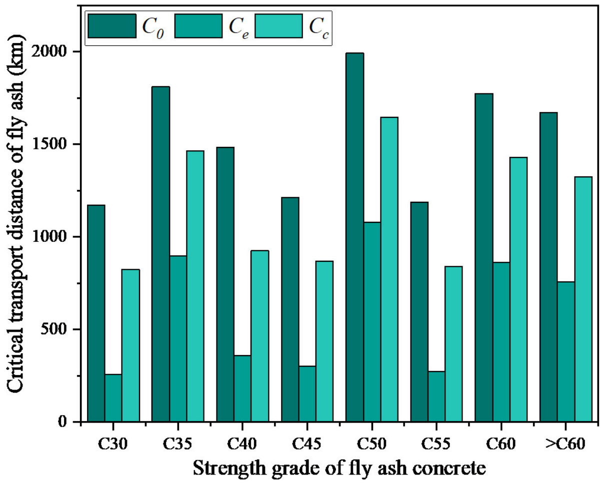

Figure 6. FAH's CTD in statistical sense. FAH: Fly ash; CTD: critical transport distance.

Table 6. Transport mode carbon emission factors [kgCO_{2eq}/(t·km)]

Transport modes	factor	Transport modes	factor
Light petrol truck transport (load 2 t): T1	0.334	Medium-sized gasoline truck transport (load 8 t): T2	0.115
Heavy petrol truck transport (10 t load): T3	0.104	Heavy gasoline truck transport (load 18 t): T4	0.104
Light diesel truck transport (load 2 t): T5	0.286	Medium-sized diesel truck transport (load 8 t): T6	0.179
Heavy diesel truck transport (load 10 t): T7	0.162	Heavy diesel truck transport (load 18 t): T8	0.129
Heavy diesel truck transport (load 30 t): T9	0.078	Heavy diesel truck transport (load 46 t): T10	0.057
Electric locomotive transport: T11	0.010	Diesel locomotive transport: T12	0.011
Rail transport (average for the Chinese market): T13	0.010	Liquid cargo ship transport (deadweight 2,000 t): T14	0.019
Dry bulk carrier transport (deadweight 2,500 t): T15	0.015	Container ship transport (deadweight 200TEU): T16	0.012

The influence of uncertainty of transport vehicles on the CTD

In addition to concrete mix proportions and FAH content, transport modes also significantly influence the CTD of FAH. Table 6 lists the carbon emission factors for various transport modes[67]. In this table, various transport modes are denoted as Ti.

When calculating the CTD of FAH using different transport modes, since the load capacities of T1 and T5 are only 2t, which are not suitable for the transport of building materials, T1 and T5 are excluded. Since the carbon emission factors of T3 and T4, as well as T11 and T13 are the same, only one of each pair is selected for calculation. The CTD values for different transport modes are then averaged across all strength grades of FAH concrete, resulting in the CTD of FAH under the C_0, C_c, and C_e allocation principles. The specific values are shown in Table 7 and Figure 7.

As indicated in Table 7, based on the allocation principles for C_0, C_c, and C_e, the maximum variations in the CTD of FAH across different transport modes reach 28,861 km, 21,623 km, and 10,450 km, respectively. Evidently, distinct transport modes significantly influence the CTD of FAH. Under the C_0, C_c, and C_e allocation principles, the CTD of FAH is highest for transport mode T13, at 30,292 km, 22,707 km, and 11,007 km, respectively, and lowest for mode T6, at 1,431 km, 1,084 km, and 557 km, respectively.

As illustrated in Figure 7, the CTD of FAH for transport modes to the right of the red dashed line (T12 to T16) is substantially higher than for those to the left, which are gasoline or diesel trucks with varying load

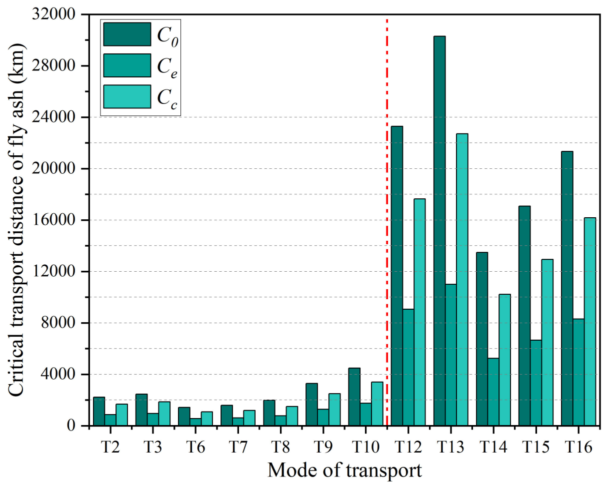

Figure 7. CTD of FAH under different transport modes. FAH: Fly ash; CTD: critical transport distance.

Table 7. CTD of FAH under different transport modes (km)

Transport modes	C_0	C_e	C_c
T2	2,227	867	1,688
T3	2,462	959	1,866
T6	1,431	557	1,084
T7	1,581	616	1,198
T8	1,985	773	1,504
T9	3,283	1,279	2,488
T10	4,493	1,750	3,405
T12	23,281	9,066	17,643
T13	30,292	11,007	22,707
T14	13,479	5,249	10,214
T15	17,073	6,648	12,938
T16	21,341	8,310	16,173
Maximum difference	28,861	10,450	21,623

The CTD values in this table are overall averages over all compressive strength grades for each transport mode, whereas Figure 6 presents compressive strength grade-specific averages for the Class 8b truck only. Hence, the T3 value in Table 7 differs from the corresponding values shown in Figure 6. CTD: Critical transport distance.

capacities. This suggests that while road transport offers advantages in convenience and flexibility, it proves to be the least effective mode for carbon reduction. For both gasoline and diesel trucks, the carbon footprint factor decreases as load capacity rises, leading to a corresponding increase in the CTD of FAH. Therefore, when road transport is necessary, trucks with higher load capacities should be used wherever road conditions permit.

When applying the C_0 allocation principle to road transport, the T10 mode yields the longest CTD for FAH at 4,493 km, while the T6 mode presents the shortest at 1,431 km-with the former being 3.14 times the latter. Under the C_c and C_e allocation principles, the CTD for FAH under the T10 mode measures 3,405 km and 1,750 km, respectively. For the T6 mode, these values are 1,084 km and 557 km, respectively. Notably, rail transport (encompassing railway, diesel locomotive, and electric locomotive transport in this study) outperforms waterway transport in carbon reduction. Consequently, the recommended hierarchy for

Table 8. Systematic comparison of different allocation approaches

Allocation principle	Basis	Key advantage	Main limitation
No allocation (C_0)	By-product bears no burden from the primary production process	Simplifies and maximizes the apparent emission-reduction benefit of IBPs	Ignores the fact that IBPs are an integral output of the production system; underestimates their true environmental burden
Mass allocation (C_m)	Mass ratio of main product to by-product	Physically clear and data-accessible	Severely overestimates the environmental burden of IBPs, discouraging their beneficial use
Traditional economic allocation (C_e)	Market prices of main product and by-product	Reflects differences in economic value	Market prices vary greatly over time and space due to supply-demand and policy shifts, leading to unstable results
System expansion	Avoided burden from substituted products	Captures system-level environmental benefits	Requires clear identification of the substituted product system; modelling can be complex
Proposed method (C_c)	Production costs of main product and by-product	Reflects real resource input, stable, and explicitly linked to the industrial chain	Production-cost data may involve confidential business information

IBP: Industrial by-product.

transport mode selection prioritizes rail, followed by waterway, and then road transport. Rational mode selection and transport structure optimization play a pivotal role in achieving carbon reduction goals, such as multimodal transportation[26].

Uncertainty in transport distance parameters

It should be noted that the material transport distances used in this study are fixed empirical values derived from typical supply chain configurations in the Chinese context [Table 1]. In practice, these distances may vary considerably depending on the geographical location of raw material sources, concrete plants, and construction sites. Such variations introduce additional uncertainty into the calculated CTD of FAH. While a comprehensive probabilistic analysis of distance parameters is beyond the scope of this study, the potential influence of transport distance uncertainty on CTD results should not be overlooked. Future research will employ Monte Carlo simulation or other uncertainty quantification techniques to systematically assess the sensitivity of CTD outcomes to variations in transport distance parameters.

Rationality and applicability of different allocation principles

The various allocation principles considered or proposed in this study each have their own theoretical applicability and limitations (See Table 8). The no-allocation principle, while simple and maximizing the apparent emission-reduction benefit of IBPs, ignores the fact that IBPs are an integral output of the production system - inconsistent with the paradigm shift from “waste” to “resource” in circular economy thinking. The mass-allocation principle, although physically clear, severely overestimates the environmental burden of IBPs, as shown in the introduction and previous studies (e.g., the carbon footprint per unit mass of FAH can exceed 400% of that of cement), which discourages IBP utilization. The traditional economic allocation reflects economic value differences, but its allocation coefficient depends heavily on fluctuating market prices (with notable temporal and spatial variability), leading to unstable and less comparable outcomes. The production-cost method proposed here captures the real resource consumption of IBPs within the production system while avoiding uncertainties caused by market price volatility; thus, it achieves a better balance between rationality and stability in allocation results.

Implications of allocation-method selection on policy and engineering practice

The results clearly demonstrate that the choice of allocation principle fundamentally affects the assessed emission-reduction contribution of IBPs. Taking the CTD as an example: under the traditional economic principle, the average CTD of FAH is only 599 km, whereas under our proposed method it reaches 1,166 km, and under no allocation it is 1,538 km. Such order-of-magnitude differences imply that using the traditional economic principle may severely underestimate the long-distance transport potential of FAH, thereby restricting its supply to wider regions and affecting the layout of low-carbon building-material industries. Therefore, a more rational and stable allocation method is a prerequisite for accurately assessing the carbon-reduction benefits of IBPs and for formulating sound regional resource-utilization policies.

CONCLUSIONS

This paper proposed a novel economic allocation principle for the environmental impacts of IBPs, based on the production costs of both the main product and the IBPs. Using life cycle assessment, it analyzed the carbon footprint characteristics of FAH concrete and FAH's CTD under different allocation principles and mix proportions. The influence of transport vehicles on CTD was further examined.

(1) A new economic allocation principle for the environmental impacts of IBPs was proposed, offering better stability than the traditional economic allocation principle. The proposed method, with appropriate case-specific adjustments, has the potential to be extended to other IBPs such as blast furnace slag and silica fume;

(2) Mix proportions significantly affect the carbon footprint and carbon footprint intensity of FAH concrete. As compressive strength increases, the carbon footprint rises while carbon footprint intensity declines, with the latter showing lower variability. Based on this carbon footprint intensity, a prediction model for the carbon footprint of FAH concrete was established;

(3) The allocation principle greatly affects the CTD of IBPs. For the Class 8b truck, the C_0 and C_e principles yield the maximum (1,538 km) and minimum (599 km) distances for FAH, respectively, a difference of up to 939 km.

(4) Under the C_0, C_c, and C_e allocation principles, rail transport (average for the Chinese market) yields the largest CTD for FAH, at 30,292 km, 22,707 km, and 11,007 km, respectively, whereas medium-sized diesel trucks (8 t load) give the smallest, at 1,431 km, 1,084 km, and 557 km;

(5) The quality of mix proportion and different transport modes can seriously affect the CTD of FAH. Regarding different transport modes, the priority selection principle is rail transport first, followed by waterway transport, and then road transport.

Based on this study, future research could focus on the following areas: (1) analyzing how different production processes of industrial main and by-products affect their carbon footprint allocation coefficients; (2) examining the influence of various development scenarios on the carbon footprint allocation coefficients of industrial by-products under the proposed principle; (3) assessing how uncertainties in cement and concrete production affect the critical transport distance of fly ash; and (4) investigating the impact of multimodal transport (road, rail, waterway) on the carbon reduction potential of fly ash concrete and its critical transport distance as infrastructure advances; (5) In addition, given the use of fixed empirical transport distances in this study, future work should incorporate probabilistic uncertainty analysis of distance parameters to further enhance the robustness of CTD assessments.

DECLARATIONS

Authors' contributions

Conceptualization: Wang, Y.; Pan, L.
Writing-original draft: Pan, L.
Supervision: Wang, Y.
Writing-review & editing: Wang, Y.; Fu, Y.
Data curation: Pan, L.; Wang, L.; Xue, S.
Formal analysis: Pan, L.; Zhang, B.; Guo, X.; Shi, C.; Liu, Y.

Methodology: Pan, L.; Fu, Y.; Zhang, B.; Guo, X.; Shi, C.
Validation: Pan, L.
Visualization: Pan, L.; Zhang, B.
Investigation: Liu, Y.; Wang, L. Fu, Y.; Liu, X.; Chang, X.
Funding acquisition: Wang, Y.

Availability of data and materials

The data and materials are available from the corresponding author upon reasonable request.

AI and AI-assisted tools statement

AI-assisted tools (Doubao-Seed 2.1 Pro, released on 2026-06-23) were used in the preparation of this manuscript solely for the creation of Figure 1, graphical abstract, and English grammar proofreading. The schematic diagram in Figure 1 and Graphic Abstract were drafted with the assistance of AI-based drawing tools to enhance visual clarity and presentation. No AI tools were used for data analysis, data interpretation, or the writing of the manuscript. All authors take full responsibility for the accuracy, integrity, and final content of the manuscript.

Financial support and sponsorship

This work was sponsored by the "Joint Scientific Research Project Funding by the National Natural Science Foundation of China and the Macao Science and Technology Development Fund (52361165660)", "National Key Research and Development Program of the 14th Five-Year Plan (2024YFC3808002)" and "Fundamental Research Special Fund for Central Public Welfare Research Institutes (2025-9047)".

Consent for publication

Not applicable.

Conflicts of interest

Guo, X. is affiliated with China Petroleum International Pipeline Co., Ltd., while the other authors have declared that they have no conflicts of interest.

Ethical approval and consent to participate

Not applicable.

Copyright

© The Author(s) 2026.

REFERENCES

1. Liu; M. R., Yang, Y.D., Yang, S.J., et al. Study on status of comprehensive utilization of fly ash. *Ind. Miner. Process.* **2021**, *50*, 45-8. DOI
2. Wu, Z.; Zhou, J.; Liang, J.; Huo, D. Comprehensive utilization of copper slag: an overview. *J. Environ. Chem. Eng.* **2026**, *14*, 121209. DOI
3. Song, Z.; Lyu, J.; Zhang, Z.; Song, B.; Liu, S.; Guan, C. Innovative application and research of industrial solid waste in mining filling materials in China. *Sustainability* **2025**, *17*, 5136. DOI
4. Zhang, L.; Zhang, F.; Tan, T. H.; et al. Valorization of industrial by-product gypsum for sustainable lightweight brick: Performance, microstructure and environmental safety assessments. *Sustainable. Chem. Pharm.* **2025**, *48*, 102179. DOI
5. Ji, G.; Li, H.; Chen, B. Modification of magnesium oxysulfate cement: a comprehensive review of industrial by-products, fibers, and functional fillers. *J. Build. Eng.* **2026**, *120*, 115430. DOI
6. Zhao, Z.; Yang, J.; Ma, Z.; Fang, W.; Liu, M.; Bi, J. Achieving urban synergistic governance of carbon, air pollution, solid waste, and water resources: lessons from 289 cities in China. *Carbon. Footprints.* **2026**, *5*, 9. DOI
7. Long, Y.; Cui, H.; Lu, Z.; Huang, B.; Wang, X.; Dou, Y. Prediction of embodied GHG emissions of building materials in Shanghai. *Carbon. Footprints.* **2024**, *3*, 12. DOI
8. Zhao, L.; Wu, D.; Hu, W.; Zhang, Z.; Yang, F.; Wang, Z. Sustainable construction material: development and evaluation of a low-carbon, industrial solid waste-based cementitious material. *J. Sustain. Metall.* **2025**, *11*, 670-81. DOI
9. Shobeiri, V.; Bennett, B.; Xie, T.; Visintin, P. A comprehensive assessment of the global warming potential of geopolymer concrete. *J. Clean. Prod.* **2021**, *297*, 126669. DOI

10. Xiao, J.; Zou, S.; Poon, C. S.; Sham, M. L.; Li, Z.; Shah, S. P. We use 30 billion tonnes of concrete each year - here's how to make it sustainable. *Nature* **2025**, *638*, 888-90. DOI
11. Echeverri, D. O.; Beltrán, V. V.; Mesa, A. P.; Ríos, L. A.; Echeverri, E. O. Financial potential of life cycle assessment of production of biofuels via hydrothermal liquefaction using microalgae in cement industry. *Energies* **2026**, *19*, 1153. DOI
12. Kim, S.; Jung, S.; Lee, J.; Jeon, D.; Kang, H.; Moon, J. Mechanochemical activation for transforming low-reactive industrial by-products to supplementary cementitious materials. *J. Sustain. Cem-Based.* **2026**, *15*, 3173-89. DOI
13. Xue, Y.; Liu, X.; Liang, Q.; Zhang, K.; Wang, Y. Synergistic utilization of multi-source industrial solid wastes in cementitious materials: a comprehensive review. *Materials. (Basel).* **2026**, *19*, 1019. DOI PubMed PMC
14. Feng, W.; Li, Z.; Yang, S.; Cui, H. Valorising industrial by-product supplementary cementitious materials for alkali-silica reaction control. *Constr. Build. Mater.* **2026**, *514*, 145522. DOI
15. Hossain, M.; Poon, C.; Dong, Y.; Xuan, D. Evaluation of environmental impact distribution methods for supplementary cementitious materials. *Renew. Sustain. Energy. Rev.* **2018**, *82*, 597-608. DOI
16. Celik, K.; Meral, C.; Petek, Gursel. A.; Mehta, P. K.; Horvath, A.; Monteiro, P. J. Mechanical properties, durability, and life-cycle assessment of self-consolidating concrete mixtures made with blended portland cements containing fly ash and limestone powder. *Cem. Concr. Compos.* **2015**, *56*, 59-72. DOI
17. Wang, J.; Wang, Y.; Sun, Y.; Tingley, D. D.; Zhang, Y. Life cycle sustainability assessment of fly ash concrete structures. *Renew. Sustain. Energy. Rev.* **2017**, *80*, 1162-74. DOI
18. Arrigoni, A.; Panesar, D. K.; Duhamel, M.; et al. Life cycle greenhouse gas emissions of concrete containing supplementary cementitious materials: cut-off *vs.* substitution. *J. Clean. Prod.* **2020**, *263*, 121465. DOI
19. Ghafoori, N.; Gbadamosi, A.; Hasnat, A. Evaluating the use of harvested fly ash as a sustainable alternative in cementitious mixtures. *Constr. Build. Mater.* **2024**, *447*, 138138. DOI
20. Singh G, Durga Prasad V. Environmental impact of concrete containing high volume fly ash and ground granulated blast furnace slag. *J. Clean. Prod.* **2024**, *448*, 141729. DOI
21. Orozco, C.; Tangtermsirikul, S.; Sugiyama, T.; Babel, S. Unraveling the environmental and economic impacts of fly ash utilization on mass concrete considering industry practices. *J. Mater. Cycles. Waste. Manag.* **2024**, *26*, 1403-17. DOI
22. Jiang, P.; Zhao, D.; Jin, C.; Ye, S.; Luan, C.; Tufail, R. F. Compressive strength prediction and low-carbon optimization of fly ash geopolymer concrete based on big data and ensemble learning. *PLoS. One.* **2024**, *19*, e0310422. DOI PubMed PMC
23. Liao, G.; Wang, D.; Wang, W.; He, Y. Microstructure, strength development mechanism, and CO_2 emission analyses of alkali-activated fly ash-slag mortars. *J. Clean. Prod.* **2024**, *442*, 141116. DOI
24. Li, Y.; Shen, J.; Lin, H.; Li, Y. Optimization design for alkali-activated slag-fly ash geopolymer concrete based on artificial intelligence considering compressive strength, cost, and carbon emission. *J. Build. Eng.* **2023**, *75*, 106929. DOI
25. Orozco, C. R.; Tangtermsirikul, S.; Sugiyama, T.; Babel, S. Comparative environmental assessment of low and high CaO fly ash in mass concrete mixtures for enhanced sustainability: Impact of fly ash type and transportation. *Environ. Res.* **2023**, *234*, 116579. DOI PubMed
26. Liu, Z. Decarbonizing freight transportation: Joint optimization of intermodal service scheduling and cargo routing. *Transp. Res. Part. C. Emerg. Technol.* **2026**, *184*, 105513. DOI
27. Jamora, J. B.; Gudia, S. E. L.; Go, A. W.; Giduquio, M. B.; Loretero, M. E. Potential CO_2 reduction and cost evaluation in use and transport of coal ash as cement replacement: a case in the Philippines. *Waste. Manag.* **2020**, *103*, 137-45. DOI PubMed
28. O'brien, K. R.; Ménaché, J.; O'moore, L. M. Impact of fly ash content and fly ash transportation distance on embodied greenhouse gas emissions and water consumption in concrete. *Int. J. Life. Cycle. Assess.* **2009**, *14*, 621-9. DOI
29. Bajpai, R.; Choudhary, K.; Srivastava, A.; Sangwan, K. S.; Singh, M. Environmental impact assessment of fly ash and silica fume based geopolymer concrete. *J. Clean. Prod.* **2020**, *254*, 120147. DOI
30. Wang, J. J. Integrated life cycle design of fly ash reinforced concrete beam based on sustainability. Ph.D. Thesis. Beijing Jiaotong University, Beijing, 2019. (in Chinese). https://kns.cnki.net/kcms2/article/abstract?v=VKKkywmE6pBcnBAAmtksNJsYXt6ZYdtbNCcf3ye5GgasAywvAOR2mdqDudZ2MR6-CFQYg_EiqZn5lRSEmOk9W-MwxLnbGrRWQfckKPR2CgIU0DitcdAOo2XpU5wrK4m-YN5KFrMJxNVNQPF3caf3LUgMyL8VgT4z5T98XuXY3Eik9W74W0eh1cz_fof451gN&uniplatform=NZKPT&language=CHS (accessed 2026-09-20).
31. Chen, C.; Habert, G.; Bouzidi, Y.; Jullien, A.; Ventura, A. LCA allocation procedure used as an incitative method for waste recycling: An application to mineral additions in concrete. *Resour. Conserv. Recy.* **2010**, *54*, 1231-40. DOI
32. Seto, K. E.; Churchill, C. J.; Panesar, D. K. Influence of fly ash allocation approaches on the life cycle assessment of cement-based materials. *J. Clean. Prod.* **2017**, *157*, 65-75. DOI
33. Hafez, H.; Kurda, R.; Cheung, W. M.; Nagaratnam, B. A systematic review of the discrepancies in life cycle assessments of green concrete. *Appl. Sci.* **2019**, *9*, 4803. DOI

34. Zhang, Y. R. Comprehensive evaluation of life cycle environmental impact of fly ash concrete. Ph.D. Thesis. Beijing Jiaotong University, Beijing. 2016. (in Chinese). https://kns.cnki.net/kcms2/article/abstract?v=VKKkywmE6pATy3vhy_QxzI3Kit-26NFGemwWTC0v4RkVWDTtcwhLzlHdE4aUx6w_xY3clSOS0R8cIey3TEIYmqYjfoxKJIo8pH2AlKFNm-HmTO8p3zA6Bx2X3CrV0D3JZe43HQmgMyta9G3TwwigdvOBnsnnCYFtqPLHezMqSj1q3uk_IfECVWgDvAne_g6S&uniplatform=NZKPT&language=CHS (accessed 2026-09-20).
35. Schepper M, Van den Heede P, Van Driessche I, De Belie N. Life cycle assessment of completely recyclable concrete. *Materials. (Basel)*. **2014**, *7*, 6010-27. DOI PubMed PMC
36. Turk, J.; Cotič, Z.; Mladenovič, A.; Šajna, A. Environmental evaluation of green concretes versus conventional concrete by means of LCA. *Waste. Manag.* **2015**, *45*, 194-205. DOI PubMed
37. Saade, M. R. M.; Silva, M. G. D.; Gomes, V. Appropriateness of environmental impact distribution methods to model blast furnace slag recycling in cement making. *Resour. Conserv. Recy.* **2015**, *99*, 40-7. DOI
38. Pan, L. Optimization design of intelligent carbon-reduction mixture ratio for fly ash concrete and whole life cycle assessment of the bridge. Ph.D. Thesis. Beijing Jiaotong University, Beijing. 2025. (in Chinese). https://kns.cnki.net/kcms2/article/abstract?v=0dH_rU7swB8g9cAEWOf0ipfQGDN8uo6gswo-nVn6XXkovsmW9Vv63h_9wsD3tW50Lqzk2glwI9titYdMWkBG_uxqKPWrIFLZBW5Rqp1fsPtcUomYZdyDbz6YAQoh0Y_6Ng-DfPfdWCee6kzXl4DxTR4dmgXX2owuOfvcsQMCq4ygdOXTOlpuPh4KCI0qyDk6 (accessed 2026-09-20).
39. Cao, J. T.; He, Y.; Wang, S. Q. Research on the link between China commodity price index and producer price index. *Price:. Theory. and. Practice.* , *2017*, 100-3. DOI
40. ISO. 2006a. ISO 14040: Environmental Management-Life Cycle Assessment-Principles and Framework. Switzerland: International Organization for Standardization. https://www.iso.org/standard/37456.html (accessed 2026-09-20).
41. ISO. 2006b. ISO 14044: Environmental Management-Life Cycle Assessment-Requirements and Guidelines. Switzerland: International Organization for Standardization. https://www.iso.org/standard/38498.html (accessed 2026-09-20).
42. Gursel, A. P. Life cycle assessment of concrete decision-support tool and case study application. University of California, Berkeley, 2014. https://webofscience.clarivate.cn/wos/alldb/full-record/PQDT:68589620 (accessed 2026-09-20).
43. Huang, L.; Liao, Q.; Yan, J.; Liang, Y.; Zhang, H. Carbon footprint of oil products pipeline transportation. *Sci. Total. Environ.* **2021**, *783*, 146906. DOI
44. Visintin, P.; Xie, T.; Bennett, B. A large-scale life-cycle assessment of recycled aggregate concrete: The influence of functional unit, emissions allocation and carbon dioxide uptake. *J. Clean. Prod.* **2020**, *248*, 119243. DOI
45. National Bureau of Statistics (NBS). China Statistical Yearbook. 2021. https://www.stats.gov.cn/sj/ndsj/2021/indexch.htm (accessed 2026-09-20).
46. Wu, A. D. Why is the empty driving rate high in China’s logistics industry. *China. Natl. Condit. Strength.* **2002**, *4*, 24. DOI
47. Cao, J.; Liu, J. F.; Zhang, W. P.; Gong, Y. F.; Zhang, C. Study on developing mechanical properties of high fly ash content concrete with age. *J Nanchang Inst Technol* 2017;36:62-6.(in Chinese) https://kns.cnki.net/kcms2/article/abstract?v=VKKkywmE6pBHO695vlTUrN0iu8-tAo2Orcyxwm_nFPpeNyBPTxPqbAXPNaBU1I-b6InSHU0mcSWJetDqTDFtkUkFq9GGs1MGnkrU0BOQXkl8Q_H4z8O_YWsR0SwFfZak6FKHBxbU4ouctRRJXm-GGTCbjzUmprK2P8VM8LLslQZ58PqfeAm52A==&uniplatform=NZKPT&language=CHS (accessed 2026-09-20).
48. Cao, Y. Research on shrinkage and cracking of fly ash concrete 20 to 70 degrees Celsius. Master Thesis. Harbin Institute of Technology, Harbin. 2011.(in Chinese) https://kns.cnki.net/kcms2/article/abstract?v=VKKkywmE6pCcuZa0N0FZ1MROMUNfFWuuuDU8uGycwkSJCXHi6fS5R9tQ2ENfXP6hInfetiwAImdZYacTfzkkMlBQbapwWpPcPW9QFpGlltK0O5u-Q_RclehWX5nGDIWb1JNSdv1sveFPCu2pWNrI81vbjNHnkPymwa528a-jbYAryQkDyS-K2g==&uniplatform=NZKPT&language=CHS (accessed 2026-09-20).
49. Chen, B.; Zhang, Y. M. Guo LP. Investigation of drying shrinkage of high volume fly ash concrete. *J Southeast Univ (Nat Sci Ed)* 2007;2:334-8.(in Chinese) https://kns.cnki.net/kcms2/article/abstract?v=VKKkywmE6pA1Wp0_0Pex8gQDDDkShA6fzBeKHU8d0ZYmiokHZARZL-CollrHRbMZlJtCnkmPrTDMZpPWVv2cMMMUX9jUYUU9Z4IqCXYXu3RMSe6RzsS0C41nyE-81ppVkZ2T-53fP865CAxNciMbVBivp2zWu-xaSaC9DLQN-XJV67BT8K2XPg==&uniplatform=NZKPT&language=CHS (accessed 2026-09-20).
50. Deng, Z. K. Experimental analysis and BP neural network prediction of strength of fly ash concrete. *Highw Traffic Technol (Appl Technol Ed)* 2011;7: 205-208.(in Chinese) https://kns.cnki.net/kcms2/article/abstract?v=VKKkywmE6pB1ZY7LmFQWc7m9BY9cOvXqyAt_binG3LmEM6qZU-0OnUaes8ZoeYAOZKJSjBuXtNgiKeh83TQIekBXEAmujkBPfizPwEfa0jyNoBC4aku493twVHkVZ_vQbUOcyXue8wjfAJi1GXaS2LaqNZL3V7P7btaYWhs9KOJugXKtPvWQXg==&uniplatform=NZKPT&language=CHS (accessed 2026-09-20).
51. Huang, C. Large quantity of fly ash concrete mechanics performance test and application. *Yangtze River* 2015;46:189-92.(in Chinese) https://kns.cnki.net/kcms2/article/abstract?v=VKKkywmE6pCX3qbxAikefXQICgB3fkYEYfW18P2hN33joKDJNYHts1uhJS5jPwOFCWnaJdVGCRsNZfpMVb2al0itPvrUMrUhBCh7H5NwjZ8bQQG-CRd27icV__uHJj2ne9yMYfINPZ-QGWOwUn_DdhHJxmVtwGw3rBfqwS-QW8yiCuEQW-fNpw==&uniplatform=NZKPT&language=CHS (accessed 2026-09-20).

52. Li, Y. Q.; Niu, D. T.; Song, H.; . Effect of multi-mineral admixtures on mechanics properties of concrete. *Concrete* 2009:47-9.(in Chinese) https://kns.cnki.net/kcms2/article/abstract?v=VKKkywmE6pCCWWBZlY2gviAQlJLPryCVhiktY090fX4mGqSlvpiNJaN4Zy1MCa5iEwY0DPmz3BNBpsl8vnwueooN1REHyf-3pudNkBVF4_nPFDFyLXyH56EhKnDJ162nS97_CjvJ7n0fwz4ItDVXz9rnX7A1ViJDfq5yi9jxOEvu1ax0CI7xJA==&uniplatform=NZKPT&language=CHS (accessed 2026-09-20).
53. Liu, X. L.; Luo, J.; Tian, B. Experimental study on influence of grade II fly ash amount on heat-releasing performance and compression strength of concrete. *Railway Eng* 2015:166-9.(in Chinese) https://kns.cnki.net/kcms2/article/abstract?v=VKKkywmE6pB3scrIb1GmJQPxZBTRnYp5qaN9wJStrYScIlSA4TTrWwGyxEVGR3Vt8gmWSvLyp2Anbn8naYNDms-1lB5g4PH6lkLnpZ5zku0Eg_aUVoC4STPT578LoI1japo2-PjI4m0Ozpzi70tTVyFw_JecdoelUWm0wUAa-YVN30nGXjde1w==&uniplatform=NZKPT&language=CHS (accessed 2026-09-20).
54. Li, G. R.; Liu, Y. Z. Study on frost resistance critical strength of high volume fly ash concrete. *Fly Ash Compr Util* 2019;2:61-4.(in Chinese) https://kns.cnki.net/kcms2/article/abstract?v=VKKkywmE6pANzO31fLpic-5HDf_lkyB51wFkgZTifWcQZTB4D7s-Wbj965aZob0Q6i4tV087JFXx5H54q3VpXiG7XFNV-QJBGK3H7u1IRCw5dqXjK_kz83ywVik0vltvrd7Eg_jRi8WNyxL4sXezmD07IPQar0uX1-WKidcVme1vkGt-6ppqeg==&uniplatform=NZKPT&language=CHS (accessed 2026-09-20).
55. Liu, S. H. Research on high fly-ash content concrete grade I and its application in deep inclined shaft lining. Master Thesis. Xinjiang Agricultural University, Urumqi, 2014.(in Chinese) https://kns.cnki.net/kcms2/article/abstract?v=VKKkywmE6pCDbz42iGlpXS4qPC-IGEomvAYspywMTLKjsp5s04i7-LQNQ7GGU_4eKbDanQ5SpmHy21b1TKAL-WZS0JlopR9Uq4c0uWcSI27KoQWyBfTfz3h5KbdJKnVPQW3ixDnBourq_13e9Y4Ilg6qBlNUAnc2vF_pekfhaDWo6aOImbMn_L1lUBqgEDuo&uniplatform=NZKPT&language=CHS (accessed 2026-09-20).
56. Liu, Y. H.; Li, C. Study on carbonization resistance of concrete with large amount of fly ash. *Henan Build Mater* 2013;6:26-7.(in Chinese) https://kns.cnki.net/kcms2/article/abstract?v=VKKkywmE6pBbGMFKXX9EoDLp9JmozcUXfWqQSz6M2cjXCNF6ruUodZ4DPQ_QVy9lNjGUfQMNY6b7bI2S8fCfQmxNMX0oEipZkQH3zJfeZ0o1faGykiHiaHDO2GYz7U3pVXAPNlUmGgxL9ljcpCK-eNm9XoNgekf-houDcavwn2wq_wKI_Xhc_A==&uniplatform=NZKPT&language=CHS (accessed 2026-09-20).
57. Niu, H. Study on high performance fly ash concrete and property prediction based on nonlinear method. Master Thesis. Shandong University of Science and Technology, Qingdao, 2005.(in Chinese) https://kns.cnki.net/kcms2/article/abstract?v=VKKkywmE6pCR0pOsjcMeg6R6AyY7KJaEV48kDS62xsuupmzsqVFB2eHDhi43xJ9vJJ2wpHMYkebJChPGkPMkObIfLIiIsXqku1AEz9ghcO7oEHsjdb3YQ4imQSsR9q4JSXAjkbQdH0vO5yB1FslOrAy-WEZWnPDC-IF2swSpIRCkYIe-LKOdNg==&uniplatform=NZKPT&language=CHS (accessed 2026-09-20).
58. Pan, L.; Wang, Y.; Li, K.; Guo, X. Predicting compressive strength of green concrete using hybrid artificial neural network with genetic algorithm. *Struct. Concr.* **2023**, *24*, 1980-96. DOI
59. Su, Y. Experimental study on hydraulic concrete with different fly ash content. *Heilongjiang Hydraul Sci Technol* 2023;51:23-6.(in Chinese) https://kns.cnki.net/kcms2/article/abstract?v=VKKkywmE6pCJA8FayGJnvUXs15uVouoCkllmu7Wz_LrAguFapyOwzeCW8pz9BlFmfZfOFATGt0-z59FtWeYbxqNSIkT-4fqjfkugVnSMk92RqNJPesvxTYk48Hr-fp1G0V3VLuWE8Cwb6d70t1plhPrTrJbdDdrHJUNCSiSp75qp1-XIHn8amw==&uniplatform=NZKPT&language=CHS (accessed 2026-09-20).
60. Tan, H. A. T.; Jiang, Z. D.; Wang, X. R. The mechanic research of high performance concrete with fly ash and furnace powder. *Bull Chin Ceram Soc* 2012;2:25-7.(in Chinese) URL:https://kns.cnki.net/kcms2/article/abstract?v=VKKkywmE6pCrD279yrZ_Jk_yzMYYI23zONMzbYQ3cd6-dGlJzXrylf70ka8AKOMm-DY4G1yZ6laUfI08yNjVzWmgXVayAjVGJPgIKs8Jos5EoON89_ks71g10kLMiqbVFSRfhG5ZlKEFMg3WLpWqzAIJb6tgm6JavzkZpt4Aiuf5xTeGKGes8w==&uniplatform=NZKPT&language=CHS (accessed 2026-09-20).
61. Wang, N. Effect of different curing conditions on carbonation resistance of fly ash concrete. Master Thesis. Zhejiang University of Technology, Hangzhou, 2014. (in Chinese) https://kns.cnki.net/kcms2/article/abstract?v=VKKkywmE6pAf8z3XdW4jVPsoisfFFOpAmkQlf-r8buum1urNq2imroRz0r412FzWaCSIBm9wugQmColIeuRRubylIyfke06q8w0rlFXXJntIaf0UGdEquSMZ0ED4VXYjdGGcotwHfVMBxnNy5kb2_3m_l_uY5wJphrV-4BhWSPGUQaCDWWh712eFUctZxxgH&uniplatform=NZKPT&language=CHS (accessed 2026-09-20).
62. Zhou, Y. Study on drying shrinkage of high volume fly ash concrete. Master Thesis. Northwest A&F University, Xianyang, 2010. (in Chinese). https://kns.cnki.net/kcms2/article/abstract?v=VKKkywmE6pCZRqd9I5K2fLz5FW6R5iIfKAwtDWH8AJV0CVs7R9BVn9q4bkEUw-ZyWH4ldjdpm7bt0k7Jd6LoXOakf4mrUAfLOfIVXyY1AyqvbCE2tnQXc0rfUlF-9Ek5Qme8CZzBnhSqzRZREEIYqsUvbaXTeOdYE3kEP8W9Yy5EgCrrKfz5Yg==&uniplatform=NZKPT&language=CHS (accessed 2026-09-20).
63. Zhang, C., 2012. Study on fly ash and cinder used as cement mixture and the influence of fly ash doage on the strength of concrete. Master Thesis. Xi’an University of Architecture and Technology, Xi’an, 2012.(in Chinese) https://kns.cnki.net/kcms2/article/abstract?v=VKKkywmE6pCThV_N02gOlg8ZSGRmSLbxYHKW_jWhyzoX8kJAt7kS70Q_Do9gbd-jw6IaAVcKcNFV9Z08PyHsvFbt9XhXoBCMO_nzwvabT9kkiK-0abMzLSpKQQFgZy9viGIlAkMJ2hNoe6g83-Pu_ObUQbvCLfTyDRmJSxEI2yUkJXwT6q63d9kY62UE_PRv&uniplatform=NZKPT&language=CHS (accessed 2026-09-20).

64. Zhou, S. Y. Experimental study on performance of mortar and concrete with high volume fly-ash. Master Thesis. North China University of Water Resources and Electric Power, Zhengzhou, 2020.(in Chinese) https://kns.cnki.net/kcms2/article/abstract?v=VKKkywmE6pA9HI_RDuj7_KcG80lGjxkMD86dXFRzP4bjj3BdJHl24m3Q8Id_WRyQ6R0WkWqOBu7zRvuGqGj0y_MEF1v7M-VOrvTsMCedD1sYy-A9ZwBqXsAwmclNfDg0_k0nPL0i_Uh4-6oFKBxhEOpC3VX_j7PaSMnouWdM-CwK6Qq56oKNP3L9AbXtjW7Q&uniplatform=NZKPT&language=CHS (accessed 2026-09-20).
65. Wang, J.; Wang, Y.; Shi, C.; Liu, Y. Strength-based life cycle CO_2 of fly ash concrete: Variation with common mix parameters. *Constr. Build. Mater.* **2024**, *411*, 134365. DOI
66. Shafigh, P.; Nomeli, M. A.; Alengaram, U. J.; Mahmud, H. B.; Jumaat, M. Z. Engineering properties of lightweight aggregate concrete containing limestone powder and high volume fly ash. *J. Clean. Prod.* **2016**, *135*, 148-57. DOI
67. Ministry of Housing and Urban-Rural Development of the People's Republic of China (MHURDPR). 2019. Building carbon emission calculation standard (GBT 51366-2019). China Construction Publishing Media Co., LTD, Beijing. http://zjj.panzhihua.gov.cn/ztzl/szsnjnljxc/4207183.shtml (accessed 2026-09-20).

Disclaimer/Publisher's Note: All statements, opinions, and data contained in this publication are solely those of the individual author(s) and contributor(s) and do not necessarily reflect those of OAE and/or the editor(s). OAE and/or the editor(s) disclaim any responsibility for harm to persons or property resulting from the use of any ideas, methods, instructions, or products mentioned in the content.

© The Author(s) 2026. Open Access This article is licensed under a Creative Commons Attribution 4.0 International License (https://creativecommons.org/licenses/by/4.0/), which permits unrestricted use, sharing, adaptation, distribution and reproduction in any medium or format, for any purpose, even commercially, as long as you give appropriate credit to the original author(s) and the source, provide a link to the Creative Commons license, and indicate if changes were made.